

# Sequestering High-Energy Electrons to Facilitate Photocatalytic Hydrogen Generation in CdSe/CdS Nanocrystals

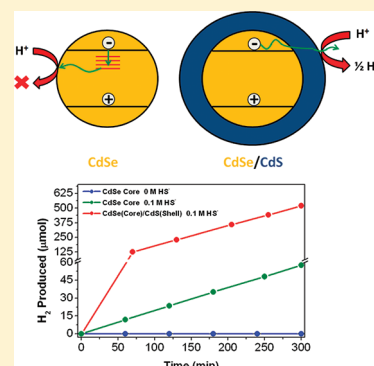
Arthur Thibert, F. Andrew Frame, Erik Busby, Michael A. Holmes, Frank E. Osterloh, and Delmar S. Larsen\*

Department of Chemistry, University of California, Davis One Shields Avenue, California 95616, United States

**S** Supporting Information

**ABSTRACT:** The photocatalytic  $\text{H}_2\text{O}$  splitting activities of CdSe and CdSe/CdS core/shell quantum dots are contrasted. CdSe/CdS core/shell quantum dots constructed from 4.0 nm CdSe quantum dots are shown to be strongly active for visible-light-driven photocatalytic  $\text{H}_2$  evolution in 0.1 M  $\text{Na}_2\text{S}/\text{Na}_2\text{SO}_3$  solution with a turnover number of 9.94 after 5 h at 103.9  $\mu\text{mol}/\text{h}$ . CdSe quantum dots themselves are only marginally active in 0.1 M  $\text{Na}_2\text{S}/\text{Na}_2\text{SO}_3$  solution with a turnover number of 1.10 after 5 h at 11.53  $\mu\text{mol}/\text{h}$ , while CdSe quantum dots in pure  $\text{H}_2\text{O}$  are found to be completely inactive. Broad-band transient absorption spectroscopy is used to elucidate the mechanisms that facilitate the enhancement in the CdSe core/shell quantum dots, which is attributed to passivation of surface-deep trap states with energies lying below the reduction potential necessary for  $\text{H}_2\text{O}$  reduction. Thus, surface trapping dynamics and energetics can be manipulated to dictate the photocatalytic activities of novel CdSe quantum dot based photocatalytic materials.

**SECTION:** Energy Conversion and Storage



The generation of  $\text{H}_2$  via photocatalytic water splitting has received considerable attention in recent years as efforts to optimize solar energy devices have accelerated.<sup>1–3</sup> Although visible photons are sufficiently energetic to split  $\text{H}_2\text{O}$  and generate high-energy  $\text{H}_2$  fuel (requiring a 1.23 eV difference of its coupled half-reactions),<sup>4</sup> materials that demonstrate this in any great yield are still not developed. This is due in part to significant overpotentials, rapid recombination of photogenerated charge carriers, poor absorption of the solar spectrum, and undesired photocorrosion reactions.<sup>5,6</sup> The recent advent of semiconductor nanoparticle technology has provided researchers with the powerful flexibility to design novel materials to address these limitations. For example, band gaps can be tuned relative to their bulk state by quantum confining photogenerated excitons to nanometer dimensions;<sup>5,7</sup> this increases the free energy (reduction potential) of charge carriers<sup>8</sup> and can exceed the  $\text{H}_2$  reduction overpotentials necessary for photocatalysis.<sup>5,9</sup> By engineering stable materials that exhibit long-living excitons at elevated free energies, efficient water splitting photocatalysis should be achievable.

Metal chalcogenides are promising materials for photocatalytic  $\text{H}_2\text{O}$  reduction because their absorption spectra strongly overlap the visible region of the solar spectrum, which eliminates the need to design complicated multicomponent sensitizer/catalyst systems.<sup>10–14</sup> While bulk CdSe is not catalytically active, the activity of CdSe nanoparticles has been theorized<sup>15–17</sup> and proven altogether with other semiconductor-based nanoparticles including ZnSe nanoribbons.<sup>18</sup> Hodges and co-workers also demonstrated that nanostructured CdSe films performed as photoanodes in a cell employing a regenerative  $\text{Na}_2\text{SeSO}_3$  electrolyte.<sup>19</sup>

Recently, we demonstrated that colloidal two-dimensional CdSe nanoribbons (NR) also exhibit photocatalytic  $\text{H}_2$  evolution in the presence of hole-scavenging  $\text{HS}^-$ , which was attributed to an increase of the band gap in quantum-confined CdSe NRs (2.7 eV) over bulk CdSe (1.74 eV).<sup>5,9,20</sup>

High-efficiency photocatalytic materials require the generation and preservation of high-energy electrons with suitable solvent access to initiate redox chemistry. This further requires the inhibition of competing mechanisms (i.e., electron/hole recombination, charge trapping, photocorrosion) that decrease catalytic activity. One approach of reducing the influence of these competing mechanisms is to design new multicomponent systems consisting of two (or more) semiconductor materials.<sup>3</sup> Such systems introduce new possibilities of manipulating electron flow from one material to the other, depending on the energy level differences of the conduction bands (for electrons) and the valence bands (for holes). For example, excitation of a semiconductor material that is in electrical contact with a second semiconductor material with a lower-energy conduction band will result in electron transport into the second material. Furthermore, if the valence band of the second material were higher in energy, then hole transport to the first material would occur. For either of these cases, the composite material is referred to as “type II” and are of significant interest in photovoltaic and electro-optical developments.<sup>21</sup>

**Received:** September 28, 2011

**Accepted:** October 6, 2011

**Published:** October 06, 2011

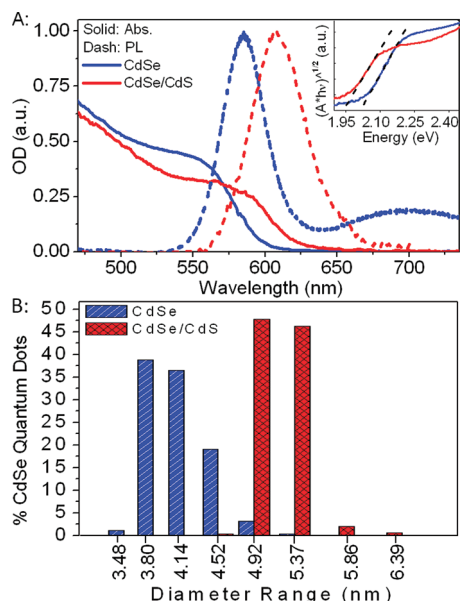


**Figure 1.** (A) Static absorption (solid lines) and photoluminescence (dashed lines) spectra of CdSe (blue lines) and CdSe/CdS core/shell QDs (red lines); (inset) Tauc plots, where the dashed lines (the  $x$ -intercepts) indicate the optical band gap for each material. (B) DLS measurements of CdSe and CdSe/CdS core/shell QDs, showing average particle sizes of 3.80 nm in  $\text{H}_2\text{O}$  and 4.92 nm in 0.1 M  $\text{HS}^-$ . This corresponds to the growth of a 2–3 monolayer CdS shell.

The isotropic CdSe/CdS core/shell nanoparticle is an important multicomponent material, but in contrast to the type-II systems described above, these QDs are type-I systems<sup>22–25</sup> with a higher-energy conduction band of the CdS shell and a low-energy valence band relative to the CdSe core. Hence, excitation of CdSe induces neither hole nor electron transport to the CdS shell, and excitation of the CdS shell (at higher energies) will rapidly transfer both holes and electrons into the inner CdSe core. Consequentially, excitation of either material results in the electrons and holes being physically removed from the surface of the QD and away from the surrounding solvent. In this Letter, we explore the photocatalytic activity of water-soluble citrate-capped CdSe quantum dots (QDs) and compare it against that of CdSe/CdS core/shell QDs synthesized from the same CdSe QD cores. The CdSe QDs (band gap of 2.01 eV) exhibit no photoactivity for  $\text{H}_2$  evolution in pure  $\text{H}_2\text{O}$  under visible light ( $\lambda > 400$  nm) and weak activity when  $\text{HS}^-$  is added. However, the activity of CdSe/CdS core/shell QDs (band gap of 1.91 eV) is 10-fold greater than that for CdSe QDs alone, despite the electrons being sequestered in the CdSe core. Thus, the primary question is how do CdSe/CdS core/shell QDs produce more  $\text{H}_2$  than CdSe QDs when the electrons must overcome a physical barrier to initiate  $\text{H}_2\text{O}$  reduction at the QD/solvent interface? To deduce this, time-dependent and excitation-intensity-dependent ultrafast transient absorption signals are used to resolve the primary dynamics that modulate the observed photoactivity.

Water-soluble citrate-capped CdSe QDs (3.80 nm) were synthesized via the protocol established by Kotov and co-workers<sup>26</sup> with aqueous cadmium perchlorate and selenourea in the presence of sodium citrate as the capping agent. The CdSe/CdS core/shell QDs were generated by mixing a stirred dispersion of CdSe QDs with 0.1 M  $\text{HS}^-$  in a 20:1 ratio (full details in Supporting Information). The formation of the CdS

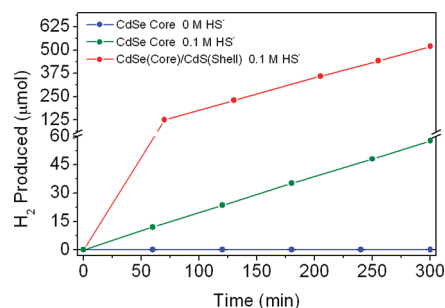


**Figure 2.** Photocatalytic hydrogen evolution for CdSe and CdSe/CdS QDs in pure  $\text{H}_2\text{O}$  and 0.1 M  $\text{HS}^-$  solution under visible light illumination from a 300 W Xe lamp equipped with a 400-nm long-pass filter. Note the change in scale of the  $y$ -axis after the break.

shell was verified by the increase of the hydrodynamic diameter of the dots from 3.80 to 4.92 nm via dynamic light scattering (DLS) measurements (Figures 1B) and by powder X-ray diffraction (Figure S11, Supporting Information), which revealed the characteristic CdS peak observed at  $29^\circ$  ( $2\theta$ ). TEM images confirm the generation of isolated CdSe QDs (Figure S11C, Supporting Information), in agreement with the DLS data.

The absorption spectra of CdSe and CdSe/CdS dots are compared in Figure 1A with band edges at 2.01 and 1.91 eV, respectively, as estimated via Tauc plots<sup>27</sup> (Figure 1A inset). Because the CdSe/CdS system is a type-I core/shell QD,<sup>23,25</sup> the CdS shell acts as a barrier that confines electrons (and holes) within the CdSe core, isolating them from the surface, which must be tunneled through before reacting with protons.<sup>28,29</sup> The small spectral red shift (70 meV) between the absorption spectra in CdSe/CdS and CdSe results from a slightly greater exciton delocalization into the CdS shell, which reduces the quantum confinement.<sup>25,29,30</sup> The QD band edge photoluminescence (PL) spectra peak at 585 and 608 nm for CdSe and CdSe/CdS QDs, respectively (Figure 1A). For the CdSe QD system, an additional red-shifted (by 0.350 eV) emission peak at 700 nm is observed that results from recombination with deeply trapped charge carriers.<sup>31–33</sup> In contrast, the PL from the CdSe/CdS QDs exhibits no deep trap emission, indicating that the CdS shell passivates the surface trap sites and, specifically, the deep traps.<sup>31,33</sup>

The photochemical  $\text{H}_2$  evolution yields under visible ( $\lambda > 400$  nm) illumination were measured and compared for (1) CdSe QDs in pure  $\text{H}_2\text{O}$ , (2) CdSe QDs in 0.1 M  $\text{HS}^-$ , and (3) CdSe/CdS QDs in 0.1 M  $\text{HS}^-$  solution (Figure 2). As expected, the CdSe QDs (blue line) produced no  $\text{H}_2$  in pure  $\text{H}_2\text{O}$  because of the rapid photocorrosion of cadmium chalcogenide materials caused by a buildup of high-energy holes in the absence of hole-scavenging species (e.g.,  $\text{HS}^-$ ).<sup>5,9</sup> Upon introduction of  $\text{HS}^-$ , the CdSe QDs (green line) exhibit significant photoactivity, producing  $11.53 \mu\text{mol H}_2/\text{h}$  over a 5 h experiment. This was enabled by the hole scavenging of the added  $\text{HS}^-$ ,<sup>34</sup> which removes high-energy holes prior to photocorrosion and hinders competing electron/hole recombination kinetics that reduce the reactive photogenerated electron population. Surprisingly, the CdSe/CdS system in  $\text{HS}^-$ , with its CdS shell physically hindering electrons from reaching the surface, exhibits a 10-fold increase in photocatalytic activity ( $103.9 \mu\text{mol H}_2/\text{h}$ ) compared to the CdSe QDs measured under identical experimental conditions (Figure 2, red curve).

Femtosecond transient absorption measurements were used to resolve the primary photoinitiated charge separation, trapping,

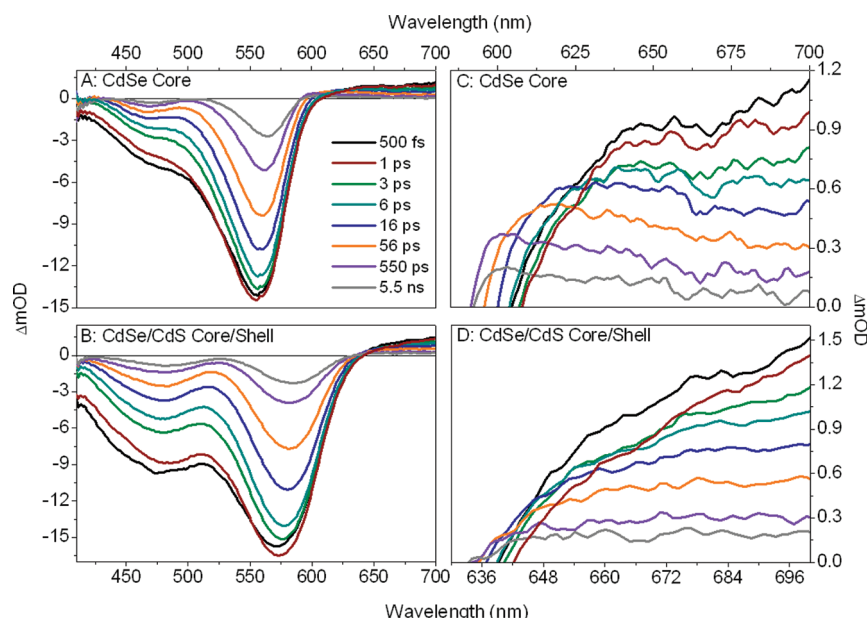


**Figure 3.** (A, B) Transient absorption spectral evolution of CdSe cores in pure  $\text{H}_2\text{O}$  and CdSe/CdS core/shells in 0.1 M  $\text{HS}^-$  excited with 400 nm pulsed light at a flux of  $14.3 \mu\text{J}/\text{pulse} \cdot \text{mm}^2$ . (C, D) Magnified depiction of the PA observed in panels A and B for  $\lambda > 600 \text{ nm}$ .

and recombination dynamics for the CdSe core and CdSe/CdS core/shell QD systems (Figure 3).<sup>9,35</sup> Immediately after 400 nm excitation, the transient spectra for both CdSe and CdSe/CdS QD systems exhibit two strong negative exciton bleaches at 475 and 560 nm that are assigned to the loss of absorption of the  $1\text{S}(\text{e})\text{-}3\text{S}_{1/2}(\text{h})$  and  $1\text{S}(\text{e})\text{-}1\text{S}_{3/2}(\text{h})$  transitions, respectively.<sup>36–38</sup> At lower probe energies ( $\lambda > 600 \text{ nm}$ ), a weak positive photoinduced absorption (PA) is resolved, which is ascribed to surface-trapped carriers.<sup>39,40</sup> Dialyzing CdSe QD cores suspended in  $\text{H}_2\text{O}$  or  $\text{H}_2\text{O}/\text{HS}^-$  increases the magnitude of the PA (Figure SI2, Supporting Information), presumably due to the removal of passivating citrate ligands that would normally be coordinated with surface Cd ions. Similar red-shifted PA features were observed by El-Sayed and co-workers in the transient spectrum of CdSe QDs upon excitation with high carrier densities ( $120\text{--}320 \mu\text{J}/\text{pulse} \cdot \text{mm}^2$ ), which were attributed to surface trapping; although biexciton contributions could not be excluded.<sup>39</sup> Klimov and co-workers also reported a PA in this spectral region for CdS nanocrystals, which was ascribed to promoting holes into deep surface traps via three-particle Auger recombination.<sup>41</sup>

We ascribe the red absorbing PA to the intraband absorption of trapped electrons below the conduction band edge into higher-lying states within the conduction band via interaction with the probe pulse. For the CdSe QD signals, the PA exhibits a well-resolved blue-shifting spectral evolution (Figure 3C). The blue shifting of the PA in the CdSe QDs then is the result of electrons migrating from shallow traps, or from the band edge, into deeper trap sites in the QD on a sub-100 ps time scale. Because no such blue shifting is observed in the CdSe/CdS core/shell QDs (Figure 3D), this process does not occur when the CdSe core QDs are passivated with a CdS shell. These interpretations complement the PL spectra in Figure 1A, whereby only deep trap emission is observed in the CdSe QD sample. The amplitude of the PA in both samples decays nonexponentially due to hole recombination including both Auger and single-electron/hole kinetics (Figure 4).<sup>16,33,35,42,43</sup>

Interestingly, the presence of the CdS shell only slightly accelerates the kinetics of the transient signals (Figure SI6, Supporting Information), which indicates that the recombination kinetics is only weakly affected by the CdS shell (other than the deep trapping kinetics discussed above); Zhang and co-workers identified similar results.<sup>44</sup> Since both trapping kinetics and recombination kinetics occur simultaneously (observed as the loss of bleach signal and PA in Figure 3A and C), a multiwavelength global analysis of the data sets is used to separate the kinetics of the two phenomena. This is accomplished within a sequential formalism that decomposes the data into time-dependent spectra (Figures 4, SI7, and SI8, Supporting Information) by fitting the data to numerical solutions of linear first-order differential equations (equation SI1, Supporting Information).<sup>45,46</sup> This approach generates difference spectra called evolutionary associated difference spectra (EADS) with time-dependent concentration profiles and provides a method to separate the trapping kinetics from recombination kinetics by evaluating their spectral properties.<sup>45,46</sup>

The extracted spectra from the global analysis resolves a fast component (300 fs) that exhibits the characteristic derivative features ascribed to a DC Stark shift resulting from multiple charge carriers (e.g., biexcitons).<sup>37</sup> Four additional populations with increasing time constants are extracted in both samples (Figure 4, legends). For the CdSe core QDs, the estimated time constants (2.6, 25, and 290 ps and 10 ns) are similar to those extracted by Weiss and co-workers on CdSe QDs via global regression analysis (1.6, 19.4, and 274 ps and 5.4 ns).<sup>47</sup> The bleach decay kinetics exhibit a narrowing on the blue side of the spectrum (Figure 4A and B), which likely involves decay of overlapping transitions between the  $1\text{S}(\text{e})\text{-}3\text{S}_{1/2}(\text{h})$  and  $1\text{S}(\text{e})\text{-}1\text{S}_{3/2}(\text{h})$  states,<sup>37</sup> which are not cleanly resolved. Comparing the extracted normalized EADS for the CdSe and CdSe/CdS QDs shows that this global analysis separates the deep trapping kinetics in the CdSe cores (Figure 4A) occurring on a 25 ps time scale from the recombination kinetics on other time scales.



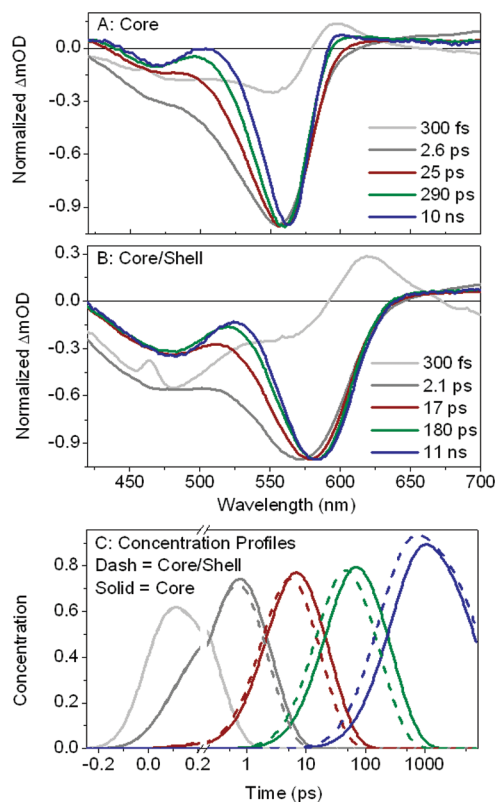


**Figure 4.** (A, B) EADS of CdSe cores in H<sub>2</sub>O and CdSe/CdS core/shells in 0.1 M HS<sup>-</sup> normalized at the lower-energy bleach. (C) Concentration profiles of CdSe cores (solid curves) and CdSe/CdS core/shells (dashed curves) after 400 nm pulsed excitation. Flux = 14.3  $\mu\text{J}/\text{pulse} \cdot \text{mm}^2$ . The 300 fs components (light-gray lines) have been scaled by 0.25 for viewing clarity of the PA at 600 nm.

To further explore the nature of the red PA and its blue-shifting kinetics, the excitation power dependence of the transient spectra at select time points was measured (Figures S, SI3, SI4, and SI5, Supporting Information). When normalized, the transient spectra for both CdSe and CdSe/CdS systems exhibit no spectral changes with increasing excitation intensity (Figures 5A and B and SI3, Supporting Information) across the spectral region of the PA. These intensity-independent spectra indicate that at these probe times, the measured spectra consist of either a homogeneous population or mixtures of populations that share an identical dependence on excitation intensity and, consequently, on the number of excitons generated by the applied excitation pulse.<sup>48</sup> Thus, the blue-shifting PA kinetics ascribed to deep electron trapping in the CdSe QD signals (Figure 5B) is not the result of a nonlinear Auger recombination mechanism similar to that observed by Klimov and co-workers in CdS nanocrystals, which would exhibit a nonlinear power dependence.<sup>41</sup>

Although spectrally homogeneous, the dependence of the amplitude of the transient spectra on the excitation intensity does address Auger recombination kinetics occurring in the samples. In both CdSe and CdSe/CdS QDs, the amplitude of the transient spectra increases monotonically with increasing excitation intensity (Figure 5C and D). This increase is linear with the increasing excitation intensity in the CdSe QDs at all three measured probe times (1.6, 15, and 100 ps). For the CdSe/CdS core/shell QDs, only the 1.6 ps spectrum exhibits a linear dependence and is nonlinear in the 15 and 100 ps transient spectra. This deviation

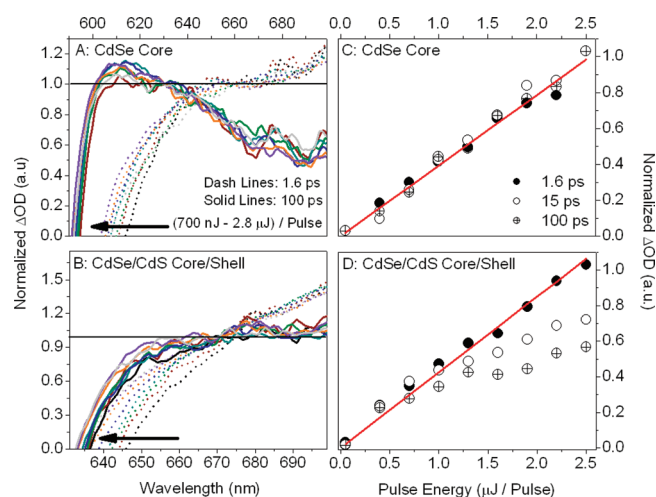
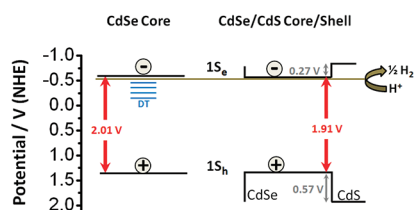


**Figure 5.** Normalized excitation-power-dependent spectra (700 nJ/pulse—2.8  $\mu\text{J}/\text{pulse}$ ) collected at 1.6 (dashed lines) and 100 ps (solid lines) for (A) CdSe QDs in pure H<sub>2</sub>O and (B) CdSe/CdS core/shell QDs in 0.1 M HS<sup>-</sup>. Black arrows in panels A and B indicate the direction of spectral evolution at 1.6 ps as the pump pulse energy is increased. Horizontal black lines in panels A and B are situated at 1  $\Delta\text{OD}$  to indicate the wavelengths at which each data set has been normalized. Core = 660 nm at 1.6 ps and 630 nm at 100 ps; core/shell = 670 nm for both 1.6 and 100 ps spectra. (C) The power dependence associated with the PA for CdSe cores exhibits a linear trend at all measured probe times. (D) CdSe/CdS core/shells exhibiting a trend characteristic of Auger recombination and scaled at the initial slope. For both CdSe and CdSe/CdS systems, the power dependence across the spectral region of the PA is independent of wavelength; red lines are linear fits through data; panels A and B and C and D use the same legend designations.

from linearity is observed at higher excitation intensities and is more pronounced at 100 ps than at 15 ps (Figure 5D). This is a characteristic signature of nonlinear Auger recombination kinetics whereby increased exciton density results in increased recombination kinetics, resulting in nonlinear excitation-dependent signals.<sup>41</sup> A linear excitation dependence indicates that the photogenerated excitons have only undergone linear (or single-exciton) dynamics (e.g., trapping or single electron–hole recombination) up to the specified probe time, thus excluding the possibility of nonlinear processes requiring multiple exciton interactions like Auger recombination. For CdSe QDs, this occurs at all probe times (Figure 5C), even at elevated excitation intensities, indicating that Auger recombination is inhibited in this system, presumably by the 400 meV deep traps that obstruct exciton mobility, which is necessary for Auger recombination. In contrast, the nonlinear dependence of the CdSe/CdS system demonstrates that passivation of these traps by the CdS shell facilitates the migration of electrons (that would otherwise be trapped) and Auger recombination on a >2 ps time scale.<sup>43</sup>

The 400 nm excitation light is resonant with both the CdSe core and the CdS shell, as demonstrated by El-Sayed and co-workers,<sup>49</sup> who also confirmed that electron-transfer kinetics from CdS to CdSe occurs on a 1–2 ps time scale. This implies that not only do both electrons and holes become sequestered in the CdSe core away from the solvent, but they also do so must faster than the time required for H<sub>2</sub> generation.<sup>34</sup> Hence, the excitation of either the CdS shell or the CdSe core has near-identical effects on both kinetics and charge localization after the first few picoseconds.

**Scheme 1.** (Left) CdSe Core Conduction ( $-0.62\text{ V}$ )<sup>7</sup> and Valence ( $+1.39\text{ V}$ ) Band Potentials Relative to the Reduction Potential of Hydrogen (gold line,  $-0.55\text{ V}$ )<sup>5</sup> at pH = 9.3 for 4 nm Cores (band gap =  $2.07\text{ V}$ ) with Unpassivated Deep Traps (DT) in Blue; (Right) CdSe/CdS Core/Shell Conduction ( $-0.59\text{ V}$ <sup>7</sup>/ $-0.86\text{ V}$ <sup>25</sup>) and Valence ( $+1.32\text{ V}$ / $+1.89\text{ V}$ <sup>25</sup>) Band Potentials Relative to the Reduction Potential of Hydrogen ( $-0.55\text{ V}$ )<sup>5</sup> at pH = 9.3 for 5 nm Core/Shells (band gap =  $2.00\text{ V}$ )<sup>a</sup>



<sup>a</sup> The removal of CdSe deep trap sites is due to the CdS shell. Band gaps were determined via Tauc plots in Figure 1A.

Theoretically, CdSe/CdS core/shell QDs should not be better photocatalysts than CdSe QDs for three primary reasons: (1) passivation via the CdS shell decreases the band gap relative to CdSe by  $\sim 100\text{ meV}$ , (2) photogenerated charge carriers migrate and become isolated in the CdSe core due to its type-I nature, and (3) the CdS shell acts as a physical barrier that hinders access of photogenerated electrons to the surface and solvent.<sup>28,29</sup> Despite these limitations, CdSe/CdS core/shells are 10-fold better at producing  $\text{H}_2$  than pure CdSe QDs under identical conditions (Figure 2). The interplay of deep trapping, passivation, and photoactivity is illustrated in Scheme 1, in which approximate energy levels related to CdSe core and CdSe/CdS QDs are compared relative to the equilibrium potential scale (y-axis, Nernst hydrogen electrode) and the reduction potential of  $\text{H}_2$  (gold line). The  $100\text{ meV}$  reduction in the CdSe core band gap via formation of the CdS shell affects both conduction and valence band levels<sup>25</sup> and was applied equally to both levels ( $50\text{ meV}$  each) as an approximation. Both PL (Figure 2A) and transient absorption spectra (Figure 4A and C) indicate a decreased occupation of electron deep trap sites that lie below the reduction potential of  $\text{H}_2$ ; upon passivation with a CdS shell, these traps are removed, forcing electrons to reside at higher-energy sites. Hence, electrons that populate deep electron trap states below the reduction potential of  $\text{H}_2$  ( $-0.41\text{ V}$  at pH = 7;  $-0.55\text{ V}$  at pH = 9.3) do not contribute to the observed  $\text{H}_2\text{O}$  reduction photoactivity. For CdSe/CdS QDs, these traps are passivated by the CdS shell, which confines electrons to the band edge or shallow traps in the CdSe core at a potential sufficient for  $\text{H}_2\text{O}$  reduction.

Although the  $400\text{ nm}$  (ultrafast data) and visible (photocatalytic activity) excitation light used in our study excites both the CdSe core and CdS shell, the type-I nature of the combined core/shell system forces the localization of the electrons and hole into the core. This sequesters the redox-active charges away from the surface, but they are not completely insulated against accessing the solvent. Recently, Wachtveitl and co-workers demonstrated that electron tunneling in CdSe/CdS core/shell QDs exists by systematically varying the CdS shell thickness and showed that electron transfer occurs from the CdSe cores to organic methylviologen ligands bound at the CdS/solvent interface; tunneling

was hindered, but not fully prevented, as the CdS shell thickness was increased.<sup>28</sup> Lian and co-workers have observed a similar tunneling dependence in CdSe/ZnS core/shell QDs.<sup>29</sup> On the basis of our measurements and these previous studies, we argue that passivation of deep CdSe trap sites via the CdS shell plays a pivotal role in  $\text{H}_2$  generation and that isolation of charge carriers to the CdSe core is not detrimental to the photoproduction of  $\text{H}_2$  because the tunneling rate of electrons is 3 orders of magnitude quicker than that required for solvent reduction.<sup>28,34</sup>

To conclude, we have demonstrated a 10-fold increase in visible-light-driven photocatalytic  $\text{H}_2$  evolution activity for CdSe/CdS core/shell QDs over CdSe core QDs alone. The photocatalytic activity enhancement is attributed to the passivation of surface-deep traps via the outer CdS shell, which maintains the photogenerated electrons at a sufficient reduction potential to reduce water. The electrons must tunnel through the CdS shell to reach the surface and initiate redox chemistry, which does not adversely hinder photoactivity because the redox time scale is significantly longer than the tunneling time scale. This work shows that surface quality is an important factor in dictating the photocatalytic activities of novel materials involving CdSe QDs.

## ■ ASSOCIATED CONTENT

**S Supporting Information.** Materials, experimental procedures, and supplementary data are discussed. This material is available free of charge via the Internet at <http://pubs.acs.org>.

## ■ AUTHOR INFORMATION

### Corresponding Author

\*E-mail: [dlarsen@ucdavis.edu](mailto:dlarsen@ucdavis.edu). Phone: (530) 754-9075.

## ■ ACKNOWLEDGMENT

Thanks and appreciation is extended to the donors of the American Chemical Society Petroleum Research Fund (48099-G6), the National Science Foundation (DMR-1035468), and the Hellman Family Foundation for support of this research. Thanks are also extended to Dr. Elizabeth C. Carroll for informative discussions.

## ■ REFERENCES

- (1) Zou, Z.; Ye, J.; Sayama, K.; Arakawa, H. Direct Splitting of Water under Visible Light Irradiation with an Oxide Semiconductor Photocatalyst. *Nature* **2001**, *414*, 625–627.
- (2) Kudo, A.; Miseki, Y. Heterogeneous Photocatalyst Materials for Water Splitting. *Chem. Soc. Rev.* **2009**, *38*, 253–278.
- (3) Osterloh, F. E. *Nanoparticle-Assembled Catalysts for Photochemical Water Splitting*; John Wiley & Sons, Ltd: New York, 2010.
- (4) Licht, S. Solar Water Splitting to Generate Hydrogen Fuel: A Photothermal Electrochemical Analysis. *Int. J. Hydrogen Energy* **2005**, *30*, 459–470.
- (5) Frame, F. A.; Osterloh, F. E. CdSe– $\text{MoS}_2$ : A Quantum Size-Confined Photocatalyst for Hydrogen Evolution from Water under Visible Light. *J. Phys. Chem. C* **2010**, *114*, 10628–10633.
- (6) Ni, M.; Leung, M. K. H.; Leung, D. Y. C.; Sumathy, K. A Review and Recent Developments in Photocatalytic Water-Splitting Using  $\text{TiO}_2$  for Hydrogen Production. *Renewable Sustainable Energy Rev.* **2007**, *11*, 401–425.
- (7) Kucur, E.; Riegler, J.; Urban, G. A.; Nann, T. Determination of Quantum Confinement in CdSe Nanocrystals by Cyclic Voltammetry. *J. Chem. Phys.* **2003**, *119*, 2333–2337.

- (8) Robel, I.; Kuno, M.; Kamat, P. V. Size-Dependent Electron Injection from Excited CdSe Quantum Dots into TiO<sub>2</sub> Nanoparticles. *J. Am. Chem. Soc.* **2007**, *129*, 4136–4137.
- (9) Frame, F. A.; Carroll, E. C.; Larsen, D. S.; Sarahan, M.; Browning, N. D.; Osterloh, F. E. First Demonstration of CdSe as a Photocatalyst for Hydrogen Evolution from Water under UV and Visible Light. *Chem. Commun.* **2008**, 2206–2208.
- (10) Buhler, N.; Meier, K.; Reber, J. F. Photochemical Hydrogen-Production with Cadmium-Sulfide Suspensions. *J. Phys. Chem.* **1984**, *88*, 3261–3268.
- (11) Tsuji, I.; Kato, H.; Kudo, A. Photocatalytic Hydrogen Evolution on ZnS–CuInS<sub>2</sub>–AgInS<sub>2</sub> Solid Solution Photocatalysts with Wide Visible Light Absorption Bands. *Chem. Mater.* **2006**, *18*, 1969–1975.
- (12) Zheng, N.; Bu, X. H.; Vu, H.; Feng, P. Y. Open-Framework Chalcogenides as Visible-Light Photocatalysts for Hydrogen Generation from Water. *Angew. Chem., Int. Ed.* **2005**, *44*, 5299–5303.
- (13) Bessekhouad, Y.; Mohammadi, M.; Trari, M. Hydrogen Photoproduction from Hydrogen Sulfide on Bi<sub>2</sub>S<sub>3</sub> Catalyst. *Sol. Energy Mater. Sol. Cells* **2002**, *73*, 339–350.
- (14) Reber, J. F.; Meier, K. Photochemical Production of Hydrogen with Zinc-Sulfide Suspensions. *J. Phys. Chem.* **1984**, *88*, 5903–5913.
- (15) Serrano, E.; Rus, G.; Garcia-Martinez, J. Nanotechnology for Sustainable Energy. *Renewable Sustainable Energy Rev.* **2009**, *13*, 2373–2384.
- (16) Zhang, J. Z. Interfacial Charge Carrier Dynamics of Colloidal Semiconductor Nanoparticles. *J. Phys. Chem. B* **2000**, *104*, 7239–7253.
- (17) Harris, C.; Kamat, P. V. Photocatalysis with CdSe Nanoparticles in Confined Media: Mapping Charge Transfer Events in the Subpicosecond to Second Timescales. *ACS Nano* **2009**, *3*, 682–690.
- (18) Xiong, S. L.; Xi, B. J.; Wang, C. M.; Xi, G. C.; Liu, X. Y.; Qian, Y. T. Solution-Phase Synthesis and High Photocatalytic Activity of Wurtzite ZnSe Ultrathin Nanobelts: A General Route to 1d Semiconductor Nanos-structured Materials. *Chemistry—Eur. J.* **2007**, *13*, 7926–7932.
- (19) Hodes, G.; Howell, I. D. J.; Peter, L. M. Nanocrystalline Photoelectrochemical Cells: A New Concept in Photovoltaic Cells. *J. Electrochem. Soc.* **1992**, *139*, 3136–3140.
- (20) Thibert, A. J.; Frame, F. A.; Busby, E.; Larsen, D. S. Primary Photodynamics of Water Solubilized Two-Dimensional CdSe Nanoribbons. *J. Phys. Chem. C* **2011**, *115*, 19647–19658.
- (21) Kim, S.; Fisher, B.; Eisler, H. J.; Bawendi, M. Type-II Quantum Dots: CdTe/CdSe(Core/Shell) and CdSe/ZnTe(Core/Shell) Heterostructures. *J. Am. Chem. Soc.* **2003**, *125*, 11466–11467.
- (22) García-Santamaría, F.; Brovelli, S.; Viswanatha, R.; Hollingsworth, J. A.; Htoon, H.; Crooker, S. A.; Klimov, V. I. Breakdown of Volume Scaling in Auger Recombination in CdSe/CdS Heteronano-crystals: The Role of the Core–Shell Interface. *Nano Lett.* **2011**, *11*, 687–693.
- (23) Brovelli, S.; Schaller, R. D.; Crooker, S. A.; García-Santamaría, F.; Chen, Y.; Viswanatha, R.; Hollingsworth, J. A.; Htoon, H.; Klimov, V. I. Nano-Engineered Electron–Hole Exchange Interaction Controls Exciton Dynamics in Core–Shell Semiconductor Nanocrystals. *Nat. Commun.* **2011**, *2*, 280.
- (24) Li, J. B.; Wang, L. W. First Principle Study of Core/Shell Structure Quantum Dots. *Appl. Phys. Lett.* **2004**, *84*, 3648–3650.
- (25) Peng, X.; Schlamp, M. C.; Kadavanich, A. V.; Alivisatos, A. P. Epitaxial Growth of Highly Luminescent CdSe/CdS Core/Shell Nanocrystals with Photostability and Electronic Accessibility. *J. Am. Chem. Soc.* **1997**, *119*, 7019–7029.
- (26) Rogach, A. L.; Nagesha, D.; Ostrander, J. W.; Giersig, M.; Kotov, N. A. “Raisin Bun”-Type Composite Spheres of Silica and Semiconductor Nanocrystals. *Chem. Mater.* **2000**, *12*, 2676–2685.
- (27) Tauc, J.; Grigorovici, R.; Vancu, A. Optical Properties and Electronic Structure of Amorphous Germanium. *Phys. Status Solidi B* **1966**, *15*, 627–637.
- (28) Dworak, L.; Matylytsky, V. V.; Breus, V. V.; Braun, M.; Basche, T.; Wachtveitl, J. Ultrafast Charge Separation at the CdSe/CdS Core/Shell Quantum Dot/Methylviologen Interface: Implications for Nanocrystal Solar Cells. *J. Phys. Chem. C* **2011**, *115*, 3949–3955.
- (29) Zhu, H. M.; Song, N. H.; Lian, T. Q. Controlling Charge Separation and Recombination Rates in CdSe/ZnS Type I Core–Shell Quantum Dots by Shell Thicknesses. *J. Am. Chem. Soc.* **2010**, *132*, 15038–15045.
- (30) Muller, J.; Lupton, J. M.; Lagoudakis, P. G.; Schindler, F.; Koeppe, R.; Rogach, A. L.; Feldmann, J.; Talapin, D. V.; Weller, H. Wave Function Engineering in Elongated Semiconductor Nanocrystals with Heterogeneous Carrier Confinement. *Nano Lett.* **2005**, *5*, 2044–2049.
- (31) Hewa-Kasakarage, N. N.; Kirsanova, M.; Nemchinov, A.; Schmall, N.; El-Khoury, P. Z.; Tarnovsky, A. N.; Zamkov, M. Radiative Recombination of Spatially Extended Excitons in (ZnSe/CdS)/CdS Heterostructured Nanorods. *J. Am. Chem. Soc.* **2009**, *131*, 1328–1334.
- (32) Lifshitz, E.; Dag, I.; Litvint, I. D.; Hodes, G. Optically Detected Magnetic Resonance Study of Electron/Hole Traps on CdSe Quantum Dot Surfaces. *J. Phys. Chem. B* **1998**, *102*, 9245–9250.
- (33) Underwood, D. F.; Kippeny, T.; Rosenthal, S. J. Ultrafast Carrier Dynamics in CdSe Nanocrystals Determined by Femtosecond Fluorescence Upconversion Spectroscopy. *J. Phys. Chem. B* **2000**, *105*, 436–443.
- (34) Chakrapani, V.; Baker, D.; Kamat, P. V. Understanding the Role of the Sulfide Redox Couple in Quantum Dot-Sensitized Solar Cells. *J. Am. Chem. Soc.* **2011**, *133*, 9607–9615.
- (35) Burda, C.; Link, S.; Mohamed, M.; El-Sayed, M. The Relaxation Pathways of CdSe Nanoparticles Monitored with Femtosecond Time-Resolution from the Visible to the IR: Assignment of the Transient Features by Carrier Quenching. *J. Phys. Chem. B* **2001**, *105*, 12286–12292.
- (36) Norris, D. J.; Bawendi, M. G. Measurement and Assignment of the Size-Dependent Optical Spectrum in CdSe Quantum Dots. *Phys. Rev. B* **1996**, *53*, 16338–16346.
- (37) Klimov, V. Spectral and Dynamical Properties of Multiexcitons in Semiconductor Nanocrystals. *Annu. Rev. Phys. Chem.* **2007**, *58*, 635–673.
- (38) Guyot-Sionnest, P.; Wehrenberg, B.; Yu, D. Intraband Relaxation in CdSe Nanocrystals and the Strong Influence of the Surface Ligands. *J. Chem. Phys.* **2005**, *123*, 7.
- (39) Burda, C.; El-Sayed, M. A. High-Density Femtosecond Transient Absorption Spectroscopy of Semiconductor Nanoparticles. A Tool to Investigate Surface Quality. *Pure Appl. Chem.* **2000**, *72*, 165–177.
- (40) Malko, A. V.; Mikhailovsky, A. A.; Petruska, M. A.; Hollingsworth, J. A.; Klimov, V. I. Interplay between Optical Gain and Photo-induced Absorption in CdSe Nanocrystals. *J. Phys. Chem. B* **2004**, *108*, 5250–5255.
- (41) Klimov, V. I.; McBranch, D. W. Auger-Process-Induced Charge Separation in Semiconductor Nanocrystals. *Phys. Rev. B* **1997**, *55*, 13173–13179.
- (42) Zhang, J. Z. Ultrafast Studies of Electron Dynamics in Semiconductor and Metal Colloidal Nanoparticles: Effects of Size and Surface. *Acc. Chem. Res.* **1997**, *30*, 423–429.
- (43) Oneil, M.; Marohn, J.; McLendon, G. Dynamics of Electron–Hole Pair Recombination in Semiconductor Clusters. *J. Phys. Chem.* **1990**, *94*, 4356–4363.
- (44) Zhang, J. Z. Ultrafast Studies of Electron Dynamics in Semiconductor and Metal Colloidal Nanoparticles: Effects of Size and Surface. *Acc. Chem. Res.* **1997**, *30*, 423–429.
- (45) Amesz, J.; Hoff, A. J.; Holzwarth, A. R. Data Analysis of Time-Resolved Measurements. In *Biophysical Techniques in Photosynthesis*; Govindjee; Amesz, J., Barber, J., Blankenship, R. E., Murata, N., Ogren, W. L., Ort, D. R., Eds.; Springer: Amsterdam, The Netherlands, 2004; Vol. 3, pp 75–92.
- (46) Van Stokkum, I. H. M.; Larsen, D. S.; van Grondelle, R. Global and Target Analysis of Time-Resolved Spectra. *Biochim. Biophys. Acta* **2004**, *1657*, 82–104.
- (47) McArthur, E. A.; Morris-Cohen, A. J.; Knowles, K. E.; Weiss, E. A. Charge Carrier Resolved Relaxation of the First Excitonic State in CdSe Quantum Dots Probed with Near-Infrared Transient Absorption Spectroscopy. *J. Phys. Chem. B* **2010**, *114*, 14514–14520.
- (48) Papagiannakis, E.; van Stokkum, I. H. M.; Vengris, M.; Cogdell, R. J.; van Grondelle, R.; Larsen, D. S. Excited-State Dynamics of

Carotenoids in Light-Harvesting Complexes. 1. Exploring the Relationship between the S1 and S\* States. *J. Phys. Chem. B* **2006**, *110*, 5727–5736.

(49) Schill, A. W.; Gaddis, C. S.; Qian, W.; El-Sayed, M. A.; Cai, Y.; Milam, V. T.; Sandhage, K. Ultrafast Electronic Relaxation and Charge-Carrier Localization in CdS/CdSe/CdS Quantum-Dot Quantum-Well Heterostructures. *Nano Lett.* **2006**, *6*, 1940–1949.